V.S. VASILEVSKY

Bogolyubov Institute for Theoretical Physics, Nat. Acad. of Sci. of Ukraine
(14b, Metrolohichna Str., Kyiv 03143, Ukraine; e-mail: VSVasilevsky@gmail.com)

MICROSCOPIC THREE-CLUSTER
DESCRIPTION OF ^{11}B AND ^{11}C NUCLEI

We investigate bound and resonance states of ^{11}B and ^{11}C. For this aim, we make use a three-cluster microscopic model which is a combination of the resonating group method and the hyperspherical harmonics Method. The model employs the basis of hyperspherical harmonics to enumerate channels and to describe the three-cluster continuum. The parameters of bound states and the nature of resonance states imbedded in the three-cluster continuum are investigated in detail.

K e y w o r d s: nuclei, three-cluster microscopic models, resonating group method, hyperspherical harmonics method.

1. Introduction

We are going to study the spectra of bound and resonance states in two mirror nuclei ^{11}B and ^{11}C within a three-cluster microscopic model. The three-cluster configurations such as

^{4}He + ^{4}He + ^{3}H,

^{4}He + ^{4}He + ^{3}He
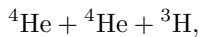
are involved in consideration. They allow us to consider the dominant two-cluster channels ^{7}Li+^{4}He and ^{7}Be+^{4}He, respectively. We restrict ourselves, by considering the bound and scattering states of ^{11}B and ^{11}C that lie below and above the three-cluster threshold ^{4}He+^{4}He+^{3}H and ^{4}He+^{4}He+^{3}He, respectively.

Nucleus ^{11}B is a very interesting object. It has ten bound states, which is unusual for nuclei of the *p*-shell. We recall that, for example, neighbor nuclei ^{12}C and ^{10}B have 2 and 5 bound states, respectively. The ground state in ^{11}B is a deeply bound state, whose energy is 11.13 MeV with respect to the three-cluster ^{4}He + ^{4}He + ^{3}H threshold or 8.88 MeV with respect to the two-cluster ^{7}Li + ^{4}He threshold. In addition, ^{11}B has very narrow resonances, the widths of two of them do not exceeds 5 eV [1]. These resonances are imbedded in the two-cluster ^{7}Li + ^{4}He continuum. There are also a large number of resonance states, which reside above the three-cluster threshold.

A similar picture is observed for ^{11}C. This nucleus has 8 bound states. Due to the Coulomb interaction,

the ground state of ^{11}C is less bound than the ground state of ^{11}B. However, it is also a deeply bound state. The ground-state energy of ^{11}C is 7.543 MeV with respect to the lowest two-cluster ^{7}Be + ^{4}He threshold and 9.13 MeV with respect to the three-cluster ^{4}He + ^{4}He + ^{3}He threshold. This nucleus, as ^{11}B, has a large set of resonance states below and above the three-cluster threshold.

Nuclei ^{11}B and ^{11}C were subjects for numerous experimental investigations [1–12]. Several microscopic methods [13–17] were applied to describe various properties of these nuclei. However, no resonance states above the three-cluster threshold were considered. The exception are works [15, 16], where the orthogonality condition model combined with the complex scaling method was used to study the resonance states in ^{11}B.

One of the main aims of the present investigation is to fill a gap in studying the properties of resonance states in the three-cluster continuum of ^{11}B and ^{11}C.

To this end, there is a quest for the Hoyle state in the literature (see, e.g., [15, 16]). Recall that the Hoyle state is a very narrow 0^+ resonance state in ^{12}C, whose width is 8.5 eV, and it lies at 0.4 MeV above the three-cluster $\alpha + \alpha + \alpha$ threshold. Hoyle suggested that the triple collision of alpha particles is a dominant way of creating ^{12}C in the Universe. Note that the nature of the Hoyle state and other resonances of ^{12}C have been investigated in [18] within the three-cluster model, which is also used in the present paper.

Within this model, we study both the bound and resonance states of ^{11}B and ^{11}C. The model, which

implements proper boundary conditions, provides the correct description of three-cluster discrete and continuous spectrum states. For the set of bound states, we calculated the parameters which determine the size and the shape of these states. The nature of resonance three-cluster states is investigated in detail. The total and partial widths of the resonance states are calculated, and the dominant decay channels for the resonances are found.

In Section 2, we briefly present our microscopic model. In Section 3, we give details of calculations and discuss properties of bound states. In this section, we also analyze the parameters of resonance states and determine the most probable ways (i.e., channels) for the decay of three-cluster resonances. Concluding remarks are presented in Section 4.

2. Model

We employ a microscopic model which is a combination of the resonating group method and hyperspherical harmonics method. This model is called the Algebraic Model with the Hyperspherical Harmonic Basis (AMHHB) [19–21], as it uses the full set of the hyperspherical harmonics to expand the many-particle wave function and to represent the Schrödinger equation in the matrix form.

The wave function of discrete and continuous-spectrum states is constructed in the form

$$\Psi^J = \widehat{\mathcal{A}}\Big\{[\Phi_1(A_1,b)\Phi_2(A_2,b)\times$$
$$\times \Phi_3(A_3,b)]_S[f_{LS}^J(\mathbf{x},\mathbf{y})]\Big\}_J, \qquad (1)$$

where $\Phi_\alpha(A_\alpha,b)$ is a shell-model wave function for the internal motion of a cluster α ($\alpha = 1,2,3$), consisted of nucleons A_α ($1 \le A_\alpha \le 4$), and $f_{LS}^J(\mathbf{x},\mathbf{y})$ is a function describing the relative motion of clusters. The relative position of clusters is determined by a a fixed set of the Jacobi vectors $\mathbf{x},\mathbf{y}$, where $\mathbf{x}$ is the Jacobi vector proportional to the distance between β and γ clusters, while $\mathbf{y}$ is a Jacobi vector connecting the α cluster to the center of mass of the β and γ clusters.

It is worth noting that the shell-model wave function $\Phi_\alpha(A_\alpha,b)$ explicitly depends on the oscillator length b. In different realizations of the many-cluster model, this parameter is used as a variational or adjustable parameter. As a rule, the oscillator length is selected to minimize the bound state energy of clusters or to reproduce their size (i.e., mass or proton root-mean-square radius). Within our model, we use the common oscillator length for all clusters involved in calculations.

In Eq. (1), we presented the function $f_{LS}^J(\mathbf{x},\mathbf{y})$ in a short form, by omitting all quantum numbers. Actually, this function has to be expanded in the states with definite values of the partial orbital momenta λ and l, associated with the Jacobi vectors $\mathbf{x}$ and $\mathbf{y}$, in the following way:

$$f_{LS}^J(\mathbf{x},\mathbf{y}) \Rightarrow \sum_{\lambda,l} f_{\lambda,l}^{(LS;J)}(x,y)\left\{Y_\lambda(\widehat{\mathbf{x}})Y_l(\widehat{\mathbf{y}})\right\}_{LM}, \quad (2)$$

where $\widehat{\mathbf{x}}$ and $\widehat{\mathbf{y}}$ are vectors of unit length. Thus, λ is the orbital momentum of the two-cluster subsystem and l is the orbital momentum related to a rotation of the third cluster around the center of mass of the two-cluster subsystem. The vector sum of the partial orbital momenta yields the total orbital momentum L. As we use the LS coupling scheme, the total angular momentum J is determined by the vector sum of the total spin S of the three-cluster system and the total orbital momentum L.

The set of functions $\left\{f_{\lambda,l}^{(LS;J)}(x,y)\right\}$ has to be determined by solving a system of coupled equations originated from the Schrödinger equation for the total wave function Ψ^J (1) with proper boundary conditions. To solve this system and to implement the necessary boundary condition, we involve the full set of hyperspherical harmonics. For this aim, we introduce the hyperspherical coordinates ρ and θ

$$x = \rho\sin\theta, \qquad y = \rho\sin\theta \qquad (3)$$

and expand the function $f_{\lambda,l}^{(LS;J)}(x,y)$ in the oscillator functions parametrized by the hyperspherical coordinates

$$f_{\lambda,l}^{(LS;J)}(x,y) = f_{\lambda,l}^{(LS;J)}(\rho,\theta) =$$
$$= \sum_{n_\rho,K} C_{n_\rho,K}^{(\lambda,l,LS;J)}\Phi_{n_\rho}^{(K)}(\rho)\chi_K^{(\lambda,l)}(\theta). \qquad (4)$$

In Refs. [19], [20], [22], one can find the definition and detailed information on hyperspherical harmonics $\chi_K^{(\lambda,l)}(\theta)$ and the function of a hyperradial excitation $\Phi_{n_\rho}^{(K)}(\rho)$. The hypermomentum K and the partial angular momenta λ and l define the three-cluster

geometry and characterize different scattering channels. These three quantum numbers along with the total orbital momentum L and the total spin S will be collectively denoted as $c = \{K; l, \lambda; L, S\}$.

Having calculated the wave function of a bound state, we can determine the three-cluster spectroscopic factor in the following way:

$$SF_{LS}^J = \sqrt{\int d\mathbf{x}d\mathbf{y} \left| f_{LS}^J (\mathbf{x}, \mathbf{y}) \right|^2}.$$

The definition of the three-cluster spectroscopic factor is similar to the definition of a two-cluster spectroscopic factor. Both of them are related to the so-called asymptotic normalization constant and explicitly demonstrate effects of the Pauli principle on the wave function of the compound systems.

To obtain additional information on the geometry of the three-cluster system in bound and resonance states, we calculate the average amplitudes of motion along the vectors $\mathbf{x}$ and $\mathbf{y}$

$$a_x = \sum_{L,S} \int d\mathbf{x}d\mathbf{y} \left| f_{LS}^J (\mathbf{x}, \mathbf{y}) \right|^2 \mathbf{x}^2,$$
$$a_y = \sum_{L,S} \int d\mathbf{x}d\mathbf{y} \left| f_{LS}^J (\mathbf{x}, \mathbf{y}) \right|^2 \mathbf{y}^2. \tag{5}$$

We also calculate the average distances between clusters by using the relations

$$r_x = a_x \sqrt{\frac{A_\beta + A_\gamma}{A_\beta A_\gamma}}, \quad r_y = a_y \sqrt{\frac{A_\alpha + A_\beta + A_\gamma}{(A_\beta + A_\gamma)}}. \tag{6}$$

These quantities determine the triangle connecting the centers of mass of interacting clusters. This definition of average distances or amplitudes (Eq. (5)) is correct for bound states only, when the total wave function is normalized by the condition

$$\left\langle \Psi^J | \Psi^J \right\rangle = 1.$$

The integrals in Eq. (5) diverge, when the wave function of continuous spectrum states is involved. However, to evaluate average distances between the clusters for resonance states, one may use only the internal part of the wave function, describing a resonance state in the many-channel model. For this aim, the internal part of the wave function has to be normalized as a bound-state function. How can the internal region of a many-channel system be defined? We

define the border of an internal region by the value of hyperradius ρ_i or the number of hyperradial excitations $n_{\rho,i}$. There are large effects of the Pauli principle and the interaction between clusters inside this region. On the border of the internal region, we match the internal part of the wave function with its asymptotic part. As a result, we obtain the wave function in the whole space and matrix elements of the scattering S matrix (see details in Refs. [19, 20]).

3. Results

To calculate the spectrum of bound and resonance states in ^{11}B and ^{11}C, we make use of the Minnesota potential (MP) [23] with IV version of the spin-orbit interaction [24]. The oscillator length b is selected to minimize the energy of the three-cluster threshold ^{4}He $+^4$He $+ ^3$H. We take $b = 1.322$ fm both for ^{11}B and ^{11}C. There is one additional parameter in the present calculations. This parameter is denoted as u and connected with odd components of the Minnesota potential (see details in [23]). There are several options for selecting the parameter u of the MP. First, one can adjust this parameter to reproduce the bound and resonance states in ^{7}Li (^{7}Be) within the two-cluster $\alpha + t$ ($\alpha + ^3$He) representation. We recall that $\alpha + t$ and $\alpha + ^3$He are dominant two-cluster subsystems in ^{11}B and ^{11}C. Second, one can find values of the parameter which reproduce the ground-state energy determined with respect to the three-cluster ^{4}He $+ ^4$He $+ ^3$H or two-cluster ^{7}Li $+ ^4$He thresholds. We use the second way and thus select $u = 0.920$. This value of u gives the bound-state energy of ^{11}B, which is very close to the experimental value. The comparison of the theoretical and experimental values of the ground-state energy will be discussed later.

To study the bound and resonance states in ^{11}B and ^{11}C, we involve all hyperspherical harmonics with $K \leq 13$ for negative-parity states and $K \leq 14$ for positive-parity states. In order to cover a large range of inter-cluster distances, where the interaction between them is strong (prominent), and to reach the asymptotic region, we take all hyperradial excitations into account in the range $0 \leq n_\rho \leq 70$. The choice of $K_{\max}$ (equals 13 or 14) and $n_{\rho \max} = 70$ is dictated by the compromise between the computational burden and the precision of calculations.

As for the three-cluster configuration ^{4}He $+^4$He$ + ^3$H (^{4}He $+ ^4$He $+ ^3$He), the total spin S of the

Table 1. **Spectrum and parameters of the bound states
in ^{11}B. Energy is in MeV accounted from the three-cluster threshold**

J^π	$\frac{3}{2}^-$	$\frac{1}{2}^-$	$\frac{5}{2}^-$	$\frac{3}{2}^-$	$\frac{1}{2}^+$	$\frac{5}{2}^+$	$\frac{3}{2}^+$
$E_{J-1/2}$, MeV	−8.598	−	−6.930	−0.307	−2.623	−2.701	−
E, MeV	−11.055	−9.646	−7.380	−5.667	−2.771	−2.749	−1.544
$W_{(J-1/2)}$	59.32	−	94.92	42.57	98.74	99.71	0.96
$W_{(J+1/2)}$	40.68	100.00	5.08	57.43	1.26	0.29	99.04
$SF_{J-1/2}$	0.5938	−	0.9070	0.4499	1.6163	1.5043	0.0258
$SF_{J+1/2}$	0.3888	1.0068	0.0563	0.5478	0.0369	0.0048	1.4300
R_m, fm	2.162	2.213	2.224	2.342	3.048	2.857	3.147
r_y, fm	2.597	2.791	2.604	2.900	5.474	4.745	5.474
r_x, fm	2.878	2.993	3.047	3.381	5.784	5.332	5.784

Table 2. **Spectrum and parameters of the bound ststes
in ^{11}C. Energy is in MeV accounted from the three-cluster threshold**

J^π	$\frac{3}{2}^-$	$\frac{1}{2}^-$	$\frac{5}{2}^-$	$\frac{3}{2}^-$	$\frac{1}{2}^+$	$\frac{5}{2}^+$	$\frac{3}{2}^+$
$E_{J-1/2}$, MeV	−6.698	−	−5.013	−	−1.152	−1.138	−
E, MeV	−9.073	−7.722	−5.446	−3.835	−1.283	−1.182	−0.098
$W_{(J-1/2)}$	59.72	−	95.06	42.39	98.85	99.75	0.94
$W_{(J+1/2)}$	40.28	100.00	4.94	57.61	1.15	0.25	99.06
$SF_{J-1/2}$	0.6013	−	0.9117	0.4517	1.623982	1.5110	0.0240
$SF_{J+1/2}$	0.3859	1.0138	0.0552	0.5518	0.0332	0.0044	1.4307
R_m, fm	2.174	2.227	2.244	2.365	3.117	2.929	3.231
r_y, fm	2.640	2.848	2.650	2.971	5.692	4.920	5.359
r_x, fm	2.904	3.021	3.083	3.433	5.838	5.471	5.944

compound system equals $1/2$ (it coincides with the spin of ^{3}H (^{3}He)), then the total angular momentum J is constructed from two values of total orbital momentum $L = J - 1/2$ and $L = J + 1/2$. There is one exception from this rule: the total angular momentum $J^\pi = 1/2^-$ can be constructed only from the total orbital momentum $L^\pi = 1^-$, because there is no negative parity state with $L^\pi = 0^-$ in the three-s-cluster systems. In the present calculations, we selected the Jacobi vector **x** to connect the center of mass of two alpha particles. Thus, the orbital momentum λ, associated with this vector, has only even values. We recall that the parity π of the three-s-cluster system is determined by the partial orbital momenta $\pi = (-1)^{l+\lambda}$, which means that the parity of a state in ^{11}B (^{11}C) is determined by the orbital momentum l of ^{3}H (^{3}He) rotation around the center of mass of two alpha particles.

In what follows, the energy of bound and resonance states are measured from the three-cluster threshold.

3.1. Bound states

Consider the parameters of bound states. To these parameters, we include the bound-state energy E, weights of different total orbital momenta in the bound-state wave function W_L, mass root-mean-square radius R_m, the spectroscopic factor for a decomposition of the compound nucleus into three clusters SF_L ($= SF^J_{L,1/2}$), and average distances between clusters r_x and r_y.

In Tables 1 and 2, we display the spectrum of bound states of ^{11}B and ^{11}C, respectively, calculated with the Minnesota potential.

To study the role of spin-orbit interaction, we show the bound-state energy $E_{J-1/2}$ (second row) obtained with only one value of total orbital momentum

Table 3. **Calculated and experimental**
spectra of bound states in ^{11}B and ^{11}C

J^π	AMHHB	Exp.	AMHHB	Exp.
$\frac{3}{2}^-$	-11.052	-11.132	-9.071	-9.130
$\frac{1}{2}^-$	-9.644	-9.007	-7.721	-7.130
$\frac{5}{2}^-$	-7.377	-6.687	-5.442	-4.812
$\frac{3}{2}^-$	-5.663	-6.111	-3.832	-4.326
$\frac{1}{2}^+$	-2.759	-4.340	-1.270	-2.652
$\frac{5}{2}^+$	-2.736	-3.846	-1.168	-2.226
$\frac{3}{2}^+$	-1.532	-3.154	-0.085	-1.631

Table 4. **Spectrum of positive and negative**
parity resonance states in ^{11}B. Energy is in MeV
and measured from the three-cluster threshold

J^π	E, MeV	Γ, keV	J^π	E, MeV	Γ, keV
$\frac{3}{2}^-$	0.755	0.581	$\frac{1}{2}^+$	0.437	15.262
	1.402	185.178		0.702	12.300
	1.756	143.716		1.597	15.949
$\frac{1}{2}^-$	1.436	374.644	$\frac{3}{2}^+$	1.147	1.498
	1.895	100.951		1.367	8.577
	2.404	450.072		1.715	41.244
$\frac{5}{2}^-$	0.583	5.140×10^{-4}	$\frac{5}{2}^+$	1.047	1.542
	1.990	32.633		1.951	40.200
	2.251	138.869		2.265	54.734
	2.905	120.456		2.748	167.613

Table 5. **Spectrum of positive and negative**
parity resonance states in ^{11}C. Energy is in MeV
and measured from the three-cluster threshold

J^π	E, MeV	Γ, keV	J^π	E, MeV	Γ, keV
$\frac{3}{2}^-$	0.805	9.929×10^{-3}	$\frac{1}{2}^+$	0.906	162.936
	1.920	105.082		1.930	59.884
	2.324	619.759		2.679	86.686
$\frac{1}{2}^-$	1.142	0.7084	$\frac{3}{2}^+$	2.268	34.250
	2.266	790.977		2.478	159.280
	3.014	366.151		2.850	115.190
$\frac{5}{2}^-$	1.897	5.771	$\frac{5}{2}^+$	1.460	0.899
	3.026	182.685		2.346	82.716
	3.491	392.962		3.179	122.748

$L = J - 1/2$, and the energy E (third row) calculated with two values of total orbital momentum. In the table, we also present the weights of $L = J - 1/2$

and $L = J + 1/2$ orbital momenta in a wave function of the J^π bound state. We recall that the coupling between states with different values of total orbital momentum is determined solely by the spin-orbit interaction. Comparing $E_{J-1/2}$ and E, we see that the total angular momentum $L = J - 1/2$ is dominant for the main part of bound states in ^{11}B and ^{11}C. This is also confirmed by the weights $W_{(J-1/2)}$ and $W_{(J+1/2)}$. There are a few bound states (e.g., second $\frac{3}{2}^-$ and first $\frac{3}{2}^+$ states), where $L = J + 1/2$ is dominant. These results indicate that the spin-orbit components play an important role in the formation of bound states in ^{11}B and ^{11}C.

The quantities r_x and r_y displayed in Tables 1 and 2 indicate that the deeply bound states are compact, as the distances between interaction clusters are small. Contrary to deeply bound states, the weakly bound states are loosely states, as the distance between two alpha particles exceeds 5 fm, and ^{3}H or ^{3}He moves off the center of mass of two alpha particles by 5 fm.

In Table 3, we compare the spectrum of bound states in ^{11}B and ^{11}C, obtained within our model, with available experimental data. Experimental data are taken from Ref. [1].

One can see that the ground states of both nuclei are very close to the experimental value. However, the first excited $\frac{1}{2}^-$ state overbound by approximately 0.6 MeV. Starting from the excited $\frac{3}{2}^-$ state, all other states are underbound. This can be attributed to the peculiarities of spin-orbit components of the Minnesota potential and partially to the size of a basis involved in calculations. Indeed, one needs a rather small basis of hyperspherical harmonics to describe a deeply bound (and, consequently, very compact) state. However, much more the hyperspherical harmonics have to be used to obtain the energy of loosely bound states with necessary precision, as it was, for example, demonstrated in Ref. [18].

The results displayed in Tables 3 show that the Coulomb interaction, which is more stronger in ^{11}C, reduces the energy of bound states by 1.5–2.0 MeV. This interaction decreases the number of bound states from 10 in ^{11}B to 8 in ^{11}C.

3.2. Three-cluster resonance states

We present now the parameters of resonance states imbedded in the three-cluster continuum. These results are obtained within the AMHHB model. In Ta-

ble 4, we display the energy and the width of resonance states in ^{11}B. The resonance states with negative and positive parities are presented in different columns.

The parameters of resonance states in ^{11}C are shown in Table 5.

The results presented in Tables 4 and 5 show that, for all values of total angular momentum, the effective barrier created by the centrifugal and Coulomb forces is very large, which accommodates three resonance states in the energy range $0 \leq E \leq 5$ MeV above the three-cluster threshold. Some of the resonances ($\frac{5}{2}^-$ in ^{11}B and $\frac{3}{2}^-$ in ^{11}C) are very narrow, as their total width is less than 10 eV. There are also many resonances (11 in ^{11}B and 7 in ^{11}C) with total width, which does not exceed 100 keV. Our model predicts the existence of wide resonance states in ^{11}B and ^{11}C in the energy range $0 \leq E \leq 5$ MeV. They are the $\frac{1}{2}^-$ resonance in ^{11}B with the total width $\Gamma = 450$ keV and the $\frac{1}{2}^-$ resonance in ^{11}C with $\Gamma = 791$ keV.

3.3. Coulomb effects

The mirror nuclei help us to understand the role of Coulomb force in the formation of bound and resonance states. The most interesting is the effect of the Coulomb repulsion on the parameters of resonance states. There are twofold effects of the forces. First, the Coulomb interaction increases the effective barrier in a three-cluster system and, thus, may reduce the width of a resonance state. Second, the Coulomb interaction reduces the effective potential well in the internal region and, consequently, may push up resonance state (by increasing the resonance energy) and simultaneously increase its width. Comparing Tables 4 and 5, we see that, for the major part of resonance states obtained within our model, the second scenario is realized. For instance, all $1/2^+$ resonances in ^{11}C have larger energy and larger width than those of such resonances in ^{11}B. The same is true for $1/2^+$, $3/2^+$, and $5/2^-$ resonances in the mirror nuclei. However, there are few resonances which realize the first scenario. Indeed, comparing two lowest resonance states with the total angular momentum $J^\pi = \frac{3}{2}^-$, we observe that the energy of the resonances in ^{11}C is a little larger than that of the resonance in ^{11}B. But their width is smaller or much more smaller. There are also some examples when both the energy and the width of reso-

nance states in ^{11}C are smaller than the corresponding values in ^{11}B (e.g., this is true for the first $1/2^-$ resonance state).

3.4. Partial widths

Our method allows us to calculate not only the total width Γ of a resonance state, but also partial widths Γ_c. (Details can be found in Ref. [21].) The partial widths determine the dominant decay channels for resonance states in a many-channel system. We recall that the total width is a sum of partial widths $\Gamma = \sum_c \Gamma_c$.

Now, we consider the partial widths of two resonance states. Partial widths are defined for two different trees of the Jacobi vectors. This is done in order to throw more light on the nature of resonance states in the three-cluster continuum.

In the first tree, we take the vector $\mathbf{x}$ as a distance between two alpha particles. This tree is used in the calculations of the spectrum and wave functions of bound and resonance states. In the second tree, we select the Jacobi vector $\mathbf{x}$ to connect the center of mass of an alpha particle and ^{3}H or ^{3}He. To this end, the first tree of the Jacobi vectors is more suitable for considering the two-cluster configuration ^{3}H$+^8$Be (^{3}He $+ ^8$Be), while the second tree is appropriate for describing the clusterization ^{4}He $+ ^7$Li (^{4}He $+ ^7$Be).

The partial widths of the $5/2^-$ resonance in ^{11}B are presented in Table 6. We see that this resonance prefers to decay through the channel, in which the hypermomentum $K = 3$, the orbital moment of two alpha particles equals $\lambda = 2$, and orbital momentum of ^{3}H $l = 1$. The $5/2^-$ resonance in ^{11}B may also decay by omitting ^{4}He and ^{3}H with the orbital momentum $\lambda = 1$ and the second alpha particle with the orbital momentum $l = 2$.

In Table 7, we display the partial decay widths for the $3/2^-$ resonance in ^{11}C. This resonance state has also one dominant channel for the decay. In first tree, the dominant channel has the following quantum numbers: hypermomentum $K = 1$, partial orbital momentum of two alpha particles $\lambda = 0$, and orbital momentum of ^{3}H $l = 1$. In the second three, the orbital momentum of relative motion of ^{4}He and ^{3}H is $\lambda = 1$, and the orbital momentum of the second alpha particle $l = 0$.

In Table 8, we display the partial decay widths for $1/2^+$ resonance in ^{11}B. One notices that this

Table 6. **Dominant decay channels for the first $5/2^-$ resonance state in ^{11}B**

		$E = 0.583$, $\Gamma = 0.5140$ eV		
i	Γ_i, eV	$\{K; l, \lambda; L\}$	Γ_i, eV	$\{K; l, \lambda; L\}$
1	0.512	$\{3; 1, 2; 2\}$	0.403	$\{3; 2, 1; 2\}$
2	0.001	$\{3; 1, 2; 2\}$	0.110	$\{3; 1, 2; 2\}$
3	0.0003	$\{3; 1, 2; 2\}$	0.0003	$\{3; 0, 3; 3\}$
Tree	^{3}H + (^{4}He + ^{4}He)		^{4}He + (^{4}He + ^{3}H)	

Table 7. **Dominant decay channels for the first $3/2^-$ resonance state in ^{11}C**

		$E = 0.805$ MeV, $\Gamma = 9.929$ eV		
i	Γ_i, eV	$\{K; l, \lambda; L\}$	Γ_i, eV	$\{K; l, \lambda; L\}$
1	9.612	$\{1; 1, 0; 1\}$	7.552	$\{1; 0, 1; 1\}$
2	0.157	$\{3; 1, 2; 2\}$	2.060	$\{1; 1, 0; 1\}$
3	0.155	$\{3; 1, 2; 1\}$	0.123	$\{3; 2, 1; 2\}$
Tree	^{3}He + (^{4}He + ^{4}He)		^{4}He + (^{4}He + ^{3}He)	

Table 8. **Dominant decay channels for the first $1/2^+$ resonance state in ^{11}B**

		$E = 0.437$ MeV, $\Gamma = 16.756$ keV		
i	Γ_i, keV	$\{K; l, \lambda; L\}$	Γ_i, keV	$\{K; l, \lambda; L\}$
1	16.756	$\{0; 0, 0; 0\}$	16.756	$\{0; 0, 0; 0\}$
2	$<10^{-8}$	$\{2; 0, 0; 0\}$	$<10^{-8}$	$\{2; 0, 0; 0\}$
3	$<10^{-10}$	$\{4; 0, 0; 0\}$	$<10^{-8}$	$\{2; 1, 1; 0\}$
Tree	^{3}He + (^{4}He + ^{4}He)		^{4}He + (^{4}He + ^{3}He)	

resonance decays with the total orbital momentum $L = 0$, the hypermomentum $K = 0$, and, thus, with $l = \lambda = 0$. This is true for both trees of the Jacobi vectors or two different types of two-body clusterization of ^{11}B. It is important to underline that the dominant channel exhausts 99.99 % of the total width. Identical results are obtained for the $1/2^+$ resonance ($E = 0.906$ MeV, $\Gamma = 162.943$ keV) in ^{11}C. A similar result is obtained for the 0^+ resonance state in ^{12}C. The Hoyle state, as was shown in Ref. [18], decays through the channel with the zero value of hypermomentum, $K = 0$.

3.5. Hoyle states

We consider the $1/2^+$ resonance states in ^{11}B and ^{11}C as main candidates to the Hoyle state. Both res-

onances are accommodated close to the three-cluster threshold: the energies of resonances are $E = 0.437$ and $E = 0.906$ MeV in ^{11}B and ^{11}C, respectively. However, these resonances are much broader ($\Gamma = 16.756$ keV and $\Gamma = 162.943$ keV) than the Hoyle state in ^{12}C ($\Gamma = 8.5$ eV). As we indicated above, there are two very narrow resonance states in ^{11}B and ^{11}C with the quantum numbers $J^\pi = \frac{5}{2}^-$ and $J^\pi = \frac{3}{2}^-$, respectively. Both resonances lie not far from the three-cluster threshold ($E = 0.583$ MeV and $E = 0.805$ MeV) and their total width ($\Gamma = 0.5140$ eV and $\Gamma = 9.929$ eV) is comparable with the width of the Hoyle state. Where is the Hoyle state true in ^{11}B and ^{11}C? To answer this question, we need more information or additional criteria for selecting the Hoyle-analog states.

Let us analyze the wave function of the Hoyle state and selected resonance states in ^{11}B and ^{11}C. To simplify this task, we calculate and display the weights of basis functions of each many-particle oscillator shell. We denote these weights as W_{sh} and define as

$$W_{\text{sh}} = \sum_{n_\rho, K \in n_{\text{sh}}} \sum_{L, S} \sum_{l, \lambda} \left| C_{n_\rho, K; , l, \lambda; LS} \right|^2 .$$

The sum over n_ρ and K involves all hyperradial and hyperangular states which satisfy the relation

$$2n_\rho + K = 2n_{\text{sh}} + K_{\min},$$

where $n_{\text{sh}} = 0, 1, 2, ...$, $K_{\min} = L_{\min}$ for the normal parity state, and $K_{\min} = L_{\min} + 1$ for abnormal parity states ($L_{\min} = J - 1/2$). Thus, W_{sh} is a function of the single variable n_{sh}.

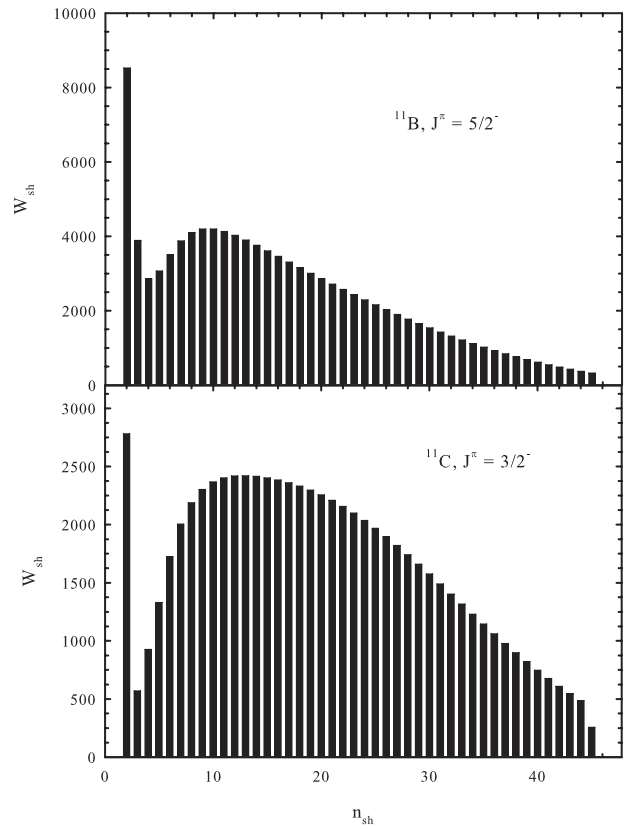First of all, we consider the weights W_{sh} for the Hoyle state in ^{12}C. They are calculated with the input parameters of Ref. [18]. One can see (Fig. 1) that the weights W_{sh} of the Hoyle state have large values, and the main contribution originates from the oscillator shells with a small value of $n_{\text{sh}} < 30$. This indicates that the Hoyle state is a compact formation. These weights will be used as additional criteria for selecting an analogue of the Hoyle state in ^{11}B and ^{11}C. Note that the wave functions of the continuous spectrum are normalized by the condition

$$\left\langle \Psi^J(E) | \Psi^J\left(\widetilde{E}\right) \right\rangle = \delta\left(k - \widetilde{k}\right),$$
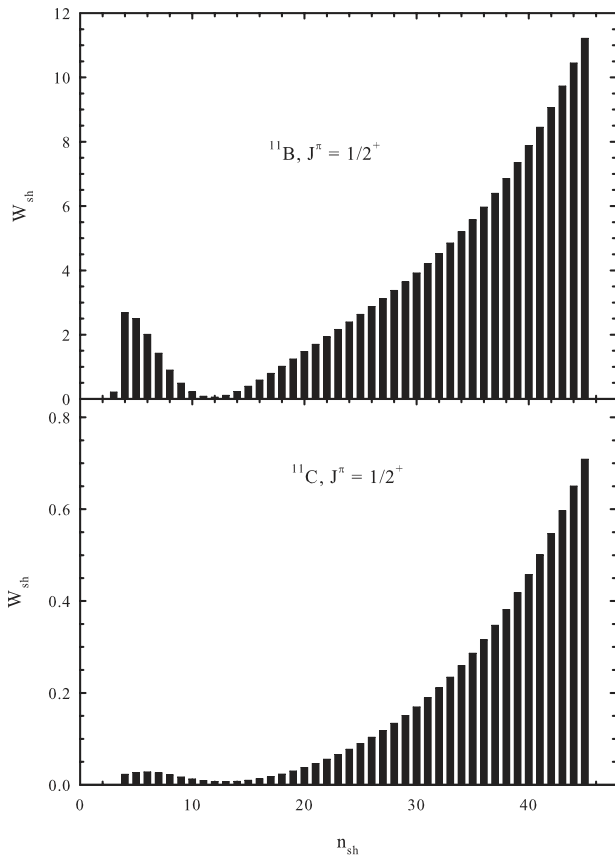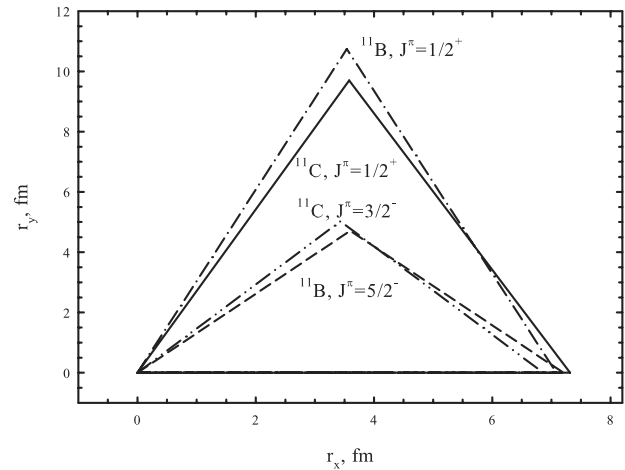
where $k = \sqrt{2mE/\hbar^2}$.
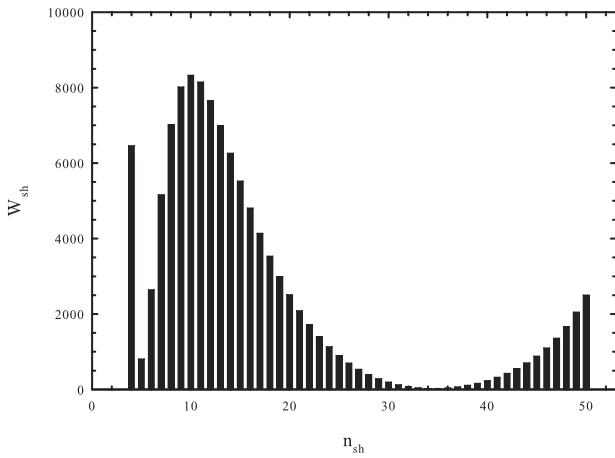
Fig. 1. Weights of the basis functions of different oscillator shells in the wave function of the 0^+ resonance state in ^{12}C

Fig. 2. Weights of various oscillator shells in the wave function of the $1/2+$ resonance state

Fig. 3. Weights of various shells in the wave function of the very narrow $5/2^-$ resonance state in ^{11}B and $3/2^-$ resonance state in ^{11}C

Fig. 4. Shape of a triangle for candidates to the Hoyle state in ^{11}B and ^{11}C

Now, we turn to the resonances in ^{11}B and ^{11}C. In Figs. 2 and 3, we display the weights of different shells in the wave function of four resonance states, which are candidates to the Hoyle state in ^{11}B and ^{11}C. As we see, the wave functions of the $1/2^+$ resonance states in these nuclei concentrate on large values of n_{sh}, which indicates that the compound nucleus is very large in this state. In addition, the weights W_{sh} are very small as compared with those of the Hoyle state in ^{12}C. Contrary to the $1/2^+$ resonance state, the $5/2^-$ resonance state in ^{11}B and the $3/2^-$ resonance state in ^{11}C have wave functions which are similar to the wave function of the Hoyle state in ^{12}C. The weights W_{sh} of these two states are very large and represented by shells with small values of n_{sh}.

By using Eqs. (5) and (6), we calculate the average distances r_x and r_y to quantify the size of a three-cluster triangle. We consider the all candidates for the Hoyle states. In Fig. 4, we show the most probable shape of a triangle connecting the center of mass of interacting clusters. We recall that r_x is the distance between two alpha particles, and r_y is a displacement of ^{3}H or ^{3}He from the center of mass of two alpha particles. One sees that the $1/2^+$ resonance states in ^{11}B and ^{11}C are very dispersed, which is in agreement with the weights of different oscillator shells in the wave function of these resonances (see Fig. 2). We note that the narrow resonance states $5/2^-$ in ^{11}B and $3/2^-$ in ^{11}C are compact states. It is worth to note that the distance between two alpha particles for all four resonance states is approximately the same and equals $r_x \approx 7$ fm, whereas the distance r_y between ^{3}H or ^{3}He and the center of mass of two alpha particles for a compact resonance is around 5 fm, and, for dispersed states, r_y is approximately 10 fm. We believe that the compact resonance states have more chance than the dispersed states to transform into a bound state of the compound nucleus.

The results presented above lead us to the conclusion that ^{11}B can be synthesized in a triple collision of clusters $\alpha + \alpha + {}^3$H with the total angular momentum $J^\pi = 5/2^-$. There is a high probability that the triple collision of two alpha particles and ^{3}He with $J^\pi = 3/2^-$ can synthesize nucleus ^{11}C.

4. Conclusions

We have studied the bound and resonance structure of ^{11}B and ^{11}C nuclei. The microscopic model, which is based on the resonating group method, provides a reasonable description of the ^{11}B and ^{11}C discrete and continuous spectrum states. We have found the optimal parameter of the nucleon-nucleon potential, which allowed us to reproduce the ground-state energy. With this potential, we obtained the correct position of other bound states of ^{11}B and ^{11}C. We have demonstrated that the spin-orbit components of the NN potential play an important role in the formation of bound and resonance states. Spectroscopic factors for a virtual decay of the bound states in ^{11}B and ^{11}C into three independent clusters are determined. They numerically manifest the effects of the Pauli principle on the wave functions of compound three-cluster systems. We calculated the parameters, which determine the shape and the size of the bound state, and investigated how they depend on the energy of the excited state.

We investigated the properties and the nature of resonance states imbedded in the three-cluster continuum. It is shown that they are generated mainly by one channel, which is weakly coupled to other channels of the three-cluster continuum.

We have discovered very narrow resonance states in ^{11}B and ^{11}C, which can be treated as an analog of the Hoyle state. The dominating decay channel for such state is revealed, and the most probable shape of a triangle connecting the center of mass of interacting clusters is determined.

1. F. Ajzenberg-Selove, Nucl. Phys. A **506**, 1 (1990).
2. N. Soić, M. Freer, L. Donadille *et al.*, Nucl. Phys. A **742**, 271 (2004).
3. N.C. Summers, S.D. Pain, N.A. Orr *et al.*, Phys. Lett. B **650**, 124 (2007).
4. T. Kawabata, H. Akimune, H. Fujita *et al.*, Nucl. Phys. A **790**, 290 (2007).
5. T. Kawabata, H. Akimune, H. Fujita *et al.*, Nucl. Phys. A **788**, 301 (2007).
6. T. Kawabata, H. Akimune, H. Fujimura *et al.*, Phys. Rev. C **70**, 034318 (2004).
7. H. Yamaguchi, T. Hashimoto, S. Hayakawa *et al.*, Phys. Rev. C **83**, 034306 (2011).
8. M. Yosoi, H. Akimune, I. Daito *et al.*, Phys. Lett. B **551**, 255 (2003).
9. H.T. Fortune and R. Sherr, Phys. Rev. C **83**, 054314 (2011).
10. M. Freer, N.L. Achouri, C. Angulo *et al.*, Phys. Rev. C **85**, 014304 (2012).
11. R.J. Charity, S.A. Komarov, L.G. Sobotka *et al.*, Phys. Rev. C **78**, 054307 (2008).

12. N. Curtis, N.I. Ashwood, W.N. Catford *et al.*, Phys. Rev. C **72**, 044320 (2005).

13. P. Descouvemont, Nucl. Phys. A **584**, 532 (1995).

14. N.K. Timofeyuk, P. Descouvemont, R.C. Johnson, Phys. Rev. C **75**, 034302 (2007).

15. T. Yamada and Y. Funaki, J. Phys. Conf. Ser. **321**, 012025 (2011).

16. T. Yamada and Y. Funaki, Phys. Rev. C **82**, 064315 (2010).

17. Y. Kanada-En'yo, T. Suhara, and F. Kobayashi, J. Phys. Conf. Ser. **321**, 012009 (2011).

18. V. Vasilevsky, F. Arickx, W. Vanroose, and J. Broeckhove, Phys. Rev. C **85**, 034318 (2012).

19. V. Vasilevsky, A.V. Nesterov, F. Arickx, and J. Broeckhove, Phys. Rev. C **63**, 034606 (2001).

20. V. Vasilevsky, A.V. Nesterov, F. Arickx, and J. Broeckhove, Phys. Rev. C **63**, 034607 (2001).

21. J. Broeckhove, F. Arickx, P. Hellinckx *et al.*, J. Phys. G Nucl. Phys. **34**, 1955 (2007).

22. V. Vasilevsky, A.V. Nesterov, F. Arickx, and J. Broeckhove, Phys. Rev. C **63**, 064604 (2001).

23. D.R. Thompson, M. LeMere, and Y.C. Tang, Nucl. Phys. A **286**, 53 (1977).

24. I. Reichstein and Y.C. Tang, Nucl. Phys. A **158**, 529 (1970).

В.С. Василевський

МІКРОСКОПІЧНИЙ ТРИКЛАСТЕРНИЙ
ОПИС ЯДЕР ^{11}B та ^{11}C

Р е з ю м е

Спектр зв'язаних та резонансних станів дзеркальних ядер ^{11}B і ^{11}C досліджено в рамках мікроскопічної трикластерної моделі, яка поєднує в собі метод резонуючих груп та метод гіперсферичних гармонік. Ця модель залучає базис гіперсферичних гармонік для нумерації каналів трикластерного континууму та реалізації необхідних граничних умов. Детально вивчено спектр зв'язаних станів ядер ^{11}B і ^{11}C та визначено параметри, які характеризують форму і розміри ядер у цих станах. Розраховано спектр резонансних станів, що занурені в трикластерний континуум $\alpha + \alpha + ^3$H і $\alpha + \alpha + ^3$He та встановлено домінуючі канали розпаду таких станів. Виявлено дуже вузькі резонанси, які є аналогом станів Хойла.